Single-particle quantum states in a one-dimensional potential well

Makito Oi, Institute of Natural Sciences, Senshu University

Abstract. In my previous report[1], which was motivated by the study of the nuclear structure of Beryllium-8 (^{8}Be) as a two-alpha-particle system, I presented a preliminary investigation of the linear rigid body from a viewpoint of the collective degrees of freedom. However, the intrinsic degrees of freedom were not treated there and remains to be investigated. For this aim, we need the details on the nuclear interactions, but they have been known to be notorious for its complexity, unlike the gravity and electromagnetic forces following the simple inverse-square law. We thus need to start our investigations with the simplified model for a description of the two-body interaction. As an initial attempt, a potential well with the finite depth is studied in this paper. In the course of study on this simplified model, an alternative approach was found, which may be more suitable for numerical applications than the standard approach known to date.

1. Introduction

The 2023 Nobel prize of Chemistry was awarded to the study of Quantum Dots[2], which is the direct application of the quantum mechanics for a potential well. The potential well had been regarded as a theoretical toy model that does not exist in reality, until the quantum dots were invented with the semiconductor materials.

The simplest case of the quantum dot can be described as a system of one fermionic particle confined in the potential well, which can be described in terms of the one-body Schrödinger equation. If a further simplicity is allowed, the equation can be reduced to one-dimensional.

$$\left\{-\frac{\hbar^2}{2\mu}\frac{d^2}{dx^2}+V(x)\right\}\Psi(x)=E\Psi(x), \tag{1}$$

where the potential well is given

$$V(x)=\begin{cases} V_0 & \cdots \quad (|x|>a), \\ 0 & \cdots \quad (|x|\leq a), \end{cases} \tag{2}$$

for $V_0>0$. In the nuclear problem, the constituent particles are confined inside the "trap" potential, called the mean field, which was self-induced through a complex mechanism of the many-body dynamics and the quantum effects[3]. In the nuclear framework, where bound states are characterised with negative energies, the potential well can be more appropriately described when the following definition is employed for the potential well,

$$V(x)=\begin{cases} 0 & \cdots \quad (|x|>a), \\ -V_0 & \cdots \quad (|x|\leq a), \end{cases} \tag{3}$$

with $V_0 > 0$. Mathematically, the two definitions of the potential well, Eqs.(2) and (3) are equivalent, but the former style is preferred by the solid-state physics (quantum dots) while the latter is by the nuclear physics. It is easy to understand that the differences in the preference come from the physical process how the potential well is produced in the relevant physics. We employ the nuclear version throughout this paper.

In the previous study [1], I regarded ^{8}Be as a two-alpha-particle system, so that the intrinsic degrees of freedom can be described with the one-body Schrödigner equation with an introduction of the reduced mass $\mu = M_\alpha/2$, where M_α is the mass of the alpha particle. By reducing the three-dimensional deviating motions of the alpha particles to the collective degrees of freedom of the linear rigid body, one may be justified to assume that the relative motions of the two particles can be simply described by the one-dimensional potential well. This approximation sounds too drastic but it may not be so badly meaningless from a physical point of view.

2. Scaling of physical quantities

In order to maximise the versatility of the present theory, the scaling is introduced for physical quantities. With the scaling, the final results can be easily applied both to quantum dots and nuclear systems, once the proper scaling factor is selected to each case.

The position variable x is scaled with the size of the potential a,

$$x = a\xi. \tag{4}$$

The scaling of energy E can be made through several steps. First of all, with an introduction of the wave number k_0, E can be written as

$$E = -E_0 = -\frac{\hbar^2 k_0^2}{2\mu}, \tag{5}$$

based on the free-particle expression for energy. It should be noted that $k_0 > 0$ is imposed. There is no mathematical reasons why negative values are prohibited for k_0, but they must be so from a physical point of view. The reasons will be provided in later discussions.

Next, the dimensionless wave number k_0' is employed as

$$k_0 = \frac{k_0 a}{a} = \frac{k_0'}{a}. \tag{6}$$

Therefore, the energy scale is given in the form of

$$E = -\frac{\hbar^2}{2\mu a^2} k_0'^2 \tag{7}$$

It should be noted that only the bound states are considered with the present energy parameterisation.

With these scaling, the Schrödinger equation reads the following expression.

$$\left\{ \frac{d^2}{d\xi^2} - \frac{2\mu a^2}{\hbar^2} V(a\xi) - (k_0 a)^2 \right\} \Psi(x) = 0, \tag{8}$$

where the potential is scaled as

$$V_0 = \frac{\hbar^2}{2\mu}(\kappa^2 + k_0^2), \tag{9}$$

or

$$V_0 = \frac{\hbar^2}{2\mu a^2}(\kappa'^2 + k_0'^2), \tag{10}$$

3. Wave functions

There are two types of wave functions in this problem: one inside the potential well and the other outside the potential well, which will be explained separately in below.

3.1 Outside the potential well

With the asymptotic requirements, the following expressions are only allowed.

$$\Psi^a(\xi) = A_a \exp(-k_0'\xi) \quad \cdots \quad (\xi > 1), \tag{11}$$

$$\Psi^c(\xi) = A_b \exp(k_0'\xi) \quad \cdots \quad (\xi < -1). \tag{12}$$

It is important to notice that the above expressions are justified only for positive k_0. If negative values are allowed, we need to modify the signature in front of k_0 so as to satisfy the asymptotic behaviours. This modification can be, however, absorbed through the redefinition of k_0', so that we can stick with the condition $k_0' > 0$ by maintaining the above mathematical expressions.

3.2 Inside the potential well

With a consideration of the parity (or the reflection symmetry), two types of functions are possible,

$$\Psi_+^b(\xi) = B_+ \cos(\kappa'\xi) \quad \cdots \quad \text{even solutions} \tag{13}$$

$$\Psi_-^b(\xi) = B_- \sin(\kappa'\xi) \quad \cdots \quad \text{odd solutions.} \tag{14}$$

In these expressions, κ' can be negative. Thanks to the symmetry properties possessed by the trigonometric functions, the effects originating from the sign of κ' can be renormalised through the redefinition of the coefficients B's. For the sake of simplicity of the theory, we should employ the condition $\kappa' > 0$, in addition to $k_0' > 0$, which is imposed above.

4. Eigenvalue equations in the standard form

The matching conditions of the wave functions and their derivatives are expressed in the form of $\frac{d\log\Psi(\xi=\pm1)}{d\xi}$, which give rise to forms of

$$k_0' = \kappa' \tan(\kappa') \quad \cdots \quad \text{even solutions} \tag{15}$$

$$k_0' = -\kappa' \cot(\kappa') \quad \cdots \quad \text{odd solutions} \tag{16}$$

As already seen in the discussion above, only the positive values for k_0' is allowed in the present theory. Therefore, the ranges for κ' are restricted so as to guarantee $k_0' > 0$.

As intersections of a circle, Eq.(9), with the curves corresponding to the above equations, the energy eigenvalues can be obtained in the form of (k_0, κ), which is usually carried out in a numerical approach.

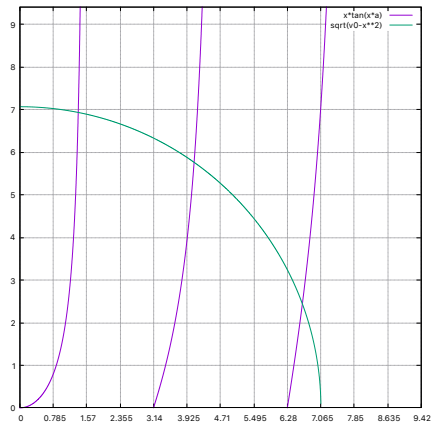

FIG. 1: Graphical evaluation of the energy eigenvalue in the standard way (the even-solution case). The abscissa and ordinate correspond to κ and k_0, respectively.

5. Extended approach for the eigenvalue equations

To simplify the expressions further, let us introduce the dimensionless potential v_0 as

$$V_0 = \frac{\hbar^2}{2\mu a^2} v_0, \tag{17}$$

where $v_0 > 0$. Then, Eq.(10) becomes

$$k_0'^2 + \kappa'^2 = v_0. \tag{18}$$

By putting Eqs.(15) and (16) into Eq.(18), we can eliminate k_0' to have equivalent equations

$$\frac{\kappa'^2}{\cos^2\kappa'} = v_0 \quad \cdots \quad \text{(even)} \tag{19}$$

$$\frac{\kappa'^2}{\sin^2\kappa'} = v_0 \quad \cdots \quad \text{(odd)} \tag{20}$$

Noting the range for κ' to be $0 < \kappa' < \sqrt{v_0}$, the above equations can be written as

$$\frac{|\cos\kappa'|}{\kappa'} = \frac{1}{\sqrt{v_0}} \quad \cdots \quad \text{(even)} \tag{21}$$

$$\frac{|\sin\kappa'|}{\kappa'} = \frac{1}{\sqrt{v_0}} \quad \cdots \quad \text{(odd)} \tag{22}$$

6. Analytical properties of even solutions

Let us first investigate the even solutions, which are given by the roots of Eq.(21). For this aim, the following function is considered.

$$f(x) = \frac{\cos x}{x}. \tag{23}$$

The zeros of this function (x_0) correspond to those of the cosine, that is,

$$x_{0,n} = \frac{2n+1}{2}\pi. \tag{24}$$

The derivative is

$$f'(x) = -\frac{1}{x^2}\left(\cos x + x\sin x\right). \tag{25}$$

The zeros of the derivative (x_1) cannot be expressed in a simple manner, but they converge to the zeros of the sine function, i.e., $n\pi$ as $x \to \infty$, that is,

$$x_{1,n} \to n\pi. \tag{26}$$

This is because the second term in the right of Eq.(25) becomes dominant as $x \to \infty$. This result implies that the extrema of $f(x)$ can be approximated with the asymptotic expression of x_1 at larger x values.

It is convenient to decompose the entire x domain (i.e., the universe), $U \equiv [0:\infty]$, into subdomains D_n, which are defined as

$$D_n, \left[n\pi : (2n+1)\frac{\pi}{2}\right], \ n = 0, 1, 2\cdots. \tag{27}$$

Obviously, $D_n \cap D_m = \varnothing$ for $n \neq m$. The direct sum of all D_n, i.e., $\bigoplus_n D_n \equiv D_A$ does not cover the whole universe U, or $D_A \subset U$. See Fig.2 for reference. It is important to notice that all the

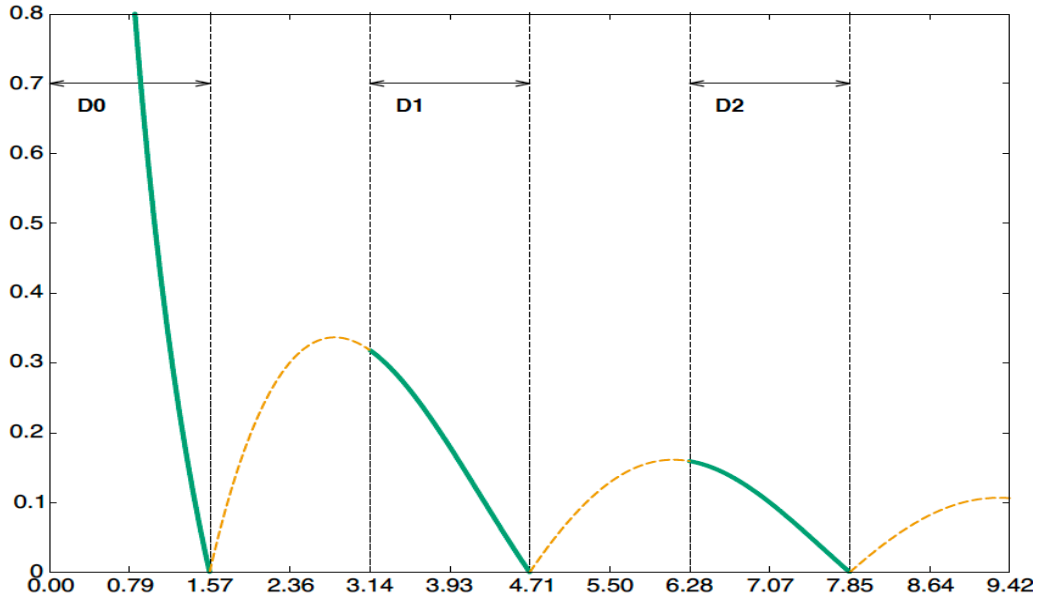

FIG. 2: Plotting of $f(x) = |\cos x|/x$ and the subdomains D_0, D_1, D_2 where the roots of $f(x) - y_0^{-1} = 0$ are possible.

domains outside of D_A, i.e., $D_A^C = U - D_A$, should be excluded from the eigenvalue calculations, because negative values are obtained for k_0' there, which can be confirmed in Eq.(15). It is possible to demonstrate that all the extrema of Eq.(23) are in the complement domain D_A^C, so that the function, Eq.(23) is a monotonically decreasing function in D_n. Consequently, the eigenvalue search can be easily done in each D_n by means of the bisection algorithm, as we see below.

Next, let us consider the solution of the equation (which corresponds to the eigenvalue equation)

$$|f(x)| - \frac{1}{y_0} = 0 \tag{28}$$

in the domain of

$$D_x \equiv [0 : y_0], \tag{29}$$

where y_0 is a given positive constant.

If $1/y_0$ is larger than the maximum in D_{n+1}, that is,

$$\frac{1}{y_0} > x_{1,n+1}, \tag{30}$$

then the roots of Eq.(28) sit only in D_k with $k < n+1$. As we prove later, positions of the maxima $x_{1,n}$ satisfy

$$x_{1,n} < n\pi, \tag{31}$$

so that function $|f(x)|$ is always monotonically decreasing in every subdomain D_n for all n. Therefore, we have n solutions when Eq.(30) holds. In this way, we can grasp perspectives of the nature of the roots for Eq.(28) without detailed numerical calculations.

1. (A solution in the ground state only):

$$\frac{1}{y_0} > |f(x_{1,1})|. \tag{32}$$

2. (Two solutions in the ground and 1st excited states):

$$\frac{1}{\pi} > \frac{1}{y_0} > |f(x_{1,2})|. \tag{33}$$

3. (n solutions in the ground and $n-1$ excited states):

$$\frac{1}{n\pi} > \frac{1}{y_0} > |f(x_{1,n+1})| \tag{34}$$

7. Numerical calculations of extrema of $f(x)$

As we already know, the roots of Eq.(25) have the asymptotic expression, Eq.(26). However, for small n such as $n = 0, 1, 2, \cdots$, the deviation from this expression cannot be negligible. Let us evaluate the values for these extrema in a numerical method.

With help of Fig.2, it is easy to guess that $f(x)$ is a monotonically decreasing function in each D_n, so that D_n contains only one root in it. This situation simplifies the numerical process to find the root in D_n by means of the bisection root-search algorithm, because the initial points can be simply set to the boundary of D_n. The numerical accuracy is set to $\epsilon = 1.0d-12$, which is sufficiently small for our purpose and close to the double precision limit in Fortran90, i.e., $1.0d-15$. As mentioned already, a code is written with Fortran90 to find numerical values for $x_1(n)$, the roots of Eq.(25) for $n = 1, 2, \cdots, 60$. Because the exact initial boundary values make the function $g(x)$ diverge, they are slightly shifted by 0.1%.

Firstly, the comparisons are made between the numerical $x_{1,n}$ and the asymptotic values $n\pi$, in terms of the relative error,

$$\Delta x = 1 - \frac{n\pi}{x_{1,n}}, \tag{35}$$

which are plotted in Fig.3.

It is possible to confirm in the numerical calculation displayed in Fig.3 that the roots $x_{1,n}$ converges slowly to the asymptotic values of $n\pi$ as n becomes larger. Agreements in the order of 10^{-3} are achieved already at and beyond $n = 10$, so that there is a temptation to approximate $x_{1,n}$ with

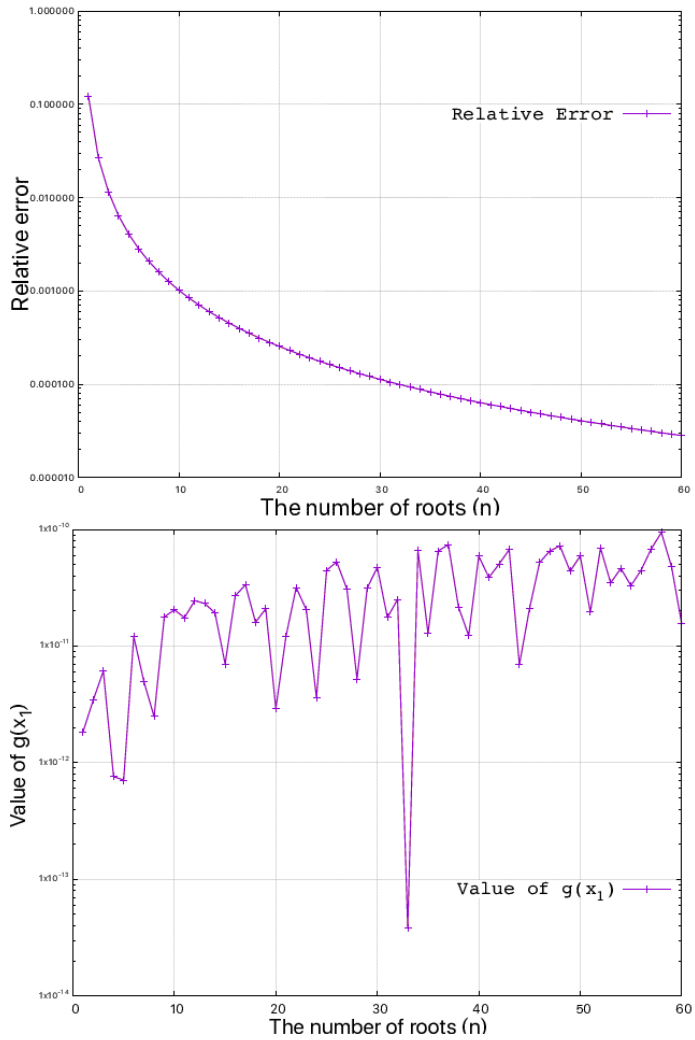

FIG. 3: Upper panel: the relative errors of the numerical results for $x_{1,n}$ with respect to the asymptotic values $(n\pi)$. Lower panel: the numerical values of $g(x_{1,n})$, which are supposed to be zero.

$n\pi$. Unfortunately, this approximation does not satisfy even the approximate condition $f'(n\pi) \simeq 0$, because $f'(n\pi) = (-1)^{n+1}/(n\pi)^2$, which cannot be negligible for small n.

In order to improve the approximation for $x_{1,n}$, let us consider the value $x_{1,n} \simeq n\pi - \delta$, where $\delta \ll 1$. We have

$$\begin{aligned} f'(n\pi-\delta) =& -(n\pi-\delta)^{-2}\{\cos(n\pi-\delta)+(n\pi-\delta)\sin(n\pi-\delta)\} \\ =& -(n\pi-\delta)^{-2}\{(-1)^n\cos\delta-(n\pi-\delta)(-1)^n\sin\delta\} \\ \simeq& (-1)^{n+1}(n\pi-\delta)^{-2}\left\{1-\frac{\delta^2}{2}+\cdots-(n\pi-\delta)(\delta-\cdots)\right\} \\ \simeq& (-1)^{n+1}(n\pi-\delta)^{-2}\left(1-n\pi\delta+\frac{\delta^2}{2}\right) \end{aligned} \tag{36}$$

Therefore, if we choose δ to satisfy

$$\delta^2 - 2n\pi\delta + 2 = 0, \tag{37}$$

then the derivative of $f(x)$ can approximately vanish. The quadratic equation for δ gives rise to

$$\delta = n\pi\left(1 \pm \sqrt{1 - \frac{2}{(n\pi)^2}}\right), \tag{38}$$

but the positive sign should be excluded to satisfy the condition $\delta \ll 1$. With the Taylor series expansion for the square root, we have an approximation for δ up to the second order,

$$\delta \simeq \frac{1}{n\pi} + \frac{1}{2}\frac{1}{(n\pi)^3} \tag{39}$$

In this way, the position of the extrema can be approximated to be

$$x_{1,n} \simeq n\pi - \frac{1}{n\pi}, \tag{40}$$

or

$$x_{1,n} \simeq n\pi - \frac{1}{n\pi} - \frac{1}{2}\frac{1}{(n\pi)^3}. \tag{41}$$

The relative errors compared with the above approximation are displayed in Fig.4, which also includes the relative errors with respect to $n\pi$ as a reference.

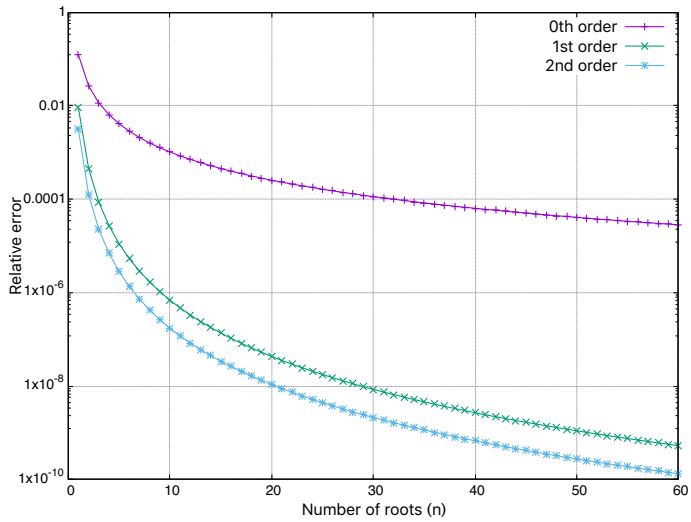

FIG. 4: Relative errors of the three types of approximated $x_1(n)$ with respect to the numerically obtained values: (i)the zero-th order ($n\pi$), (ii)the first order, Eq.(40) and (iii) the second order, Eq.(41).

With this approximate expressions for $x_{1,n}$, we have a relation

$$x_{1,n} < n\pi < x_{0,n+1}, \tag{42}$$

1	2	3	4	5
2.7983860457832299	6.1212504668986307	9.3178664617917200	12.486454395223721	15.644128370332982
2.8232827674060026	6.1240303640876910	9.3186746653747825	12.486793142813225	15.644301290712207
2.8071570001894028	6.1220146431856159	9.3180774147371306	12.486541177700465	15.644172284574474

TABLE I: Numerical values for $x_{1,n}$ for $n = 1, 2, 3, 4, 5$ (upper row), and the approximations, Eq.(40) (middle row) and Eq.(41) (bottom row).

6	7	8	9	10
18.796404366209515	21.945612879981269	25.092910412112197	28.238936575259643	31.384074017890509
18.796504273841460	21.945675734245153	25.092952492945372	28.238966117176606	31.384095547279554
18.796429617511755	21.945628720346562	25.092920997306276	28.238943996782620	31.384079421512336

TABLE II: Numerical values for $x_{1,n}$ for $n = 6, 7, 8, 9, 10$ (upper row), and the approximations, Eq.(40) (middle row) and Eq.(41) (bottom row).

which implies the monotonic decrease of $f(x)$ in D_n.

If the numerical accuracy can be compromised to the single precision, then the approximation, Eq.(40), is practically effective beyond $n = 10$. For the sake of later usages in programming, let us quote the calculated zeros for less than $n = 10$ in the tables below.

Let us finally confirm whether the numerically obtained values correspond to the extrema of the function $f(x)$, Eq.(23). In Fig.5, the graph of Eq.(23) is superposed with the points of extrema obtained both by the numerical calculations and the approximation, Eq.(40). As far as naked-eyes observation is concerned, there is no significant differences between the "exact" numerical values and the approximated values: both reproduce the extremum positions fairly well.

8. Eigenvalues of even solutions

With the preparations so far, the eigenvalue equation, Eq.(28), can be finally solved under the condition,

$$0 < x < y_0. \tag{43}$$

Let us begin with the ground-state energy and then proceed to the excited states.

8.1 Ground state

The potential well allows only one eigenstate (i.e., the ground state) if

$$\frac{1}{y_0} > f(x_{1,1}) \tag{44}$$

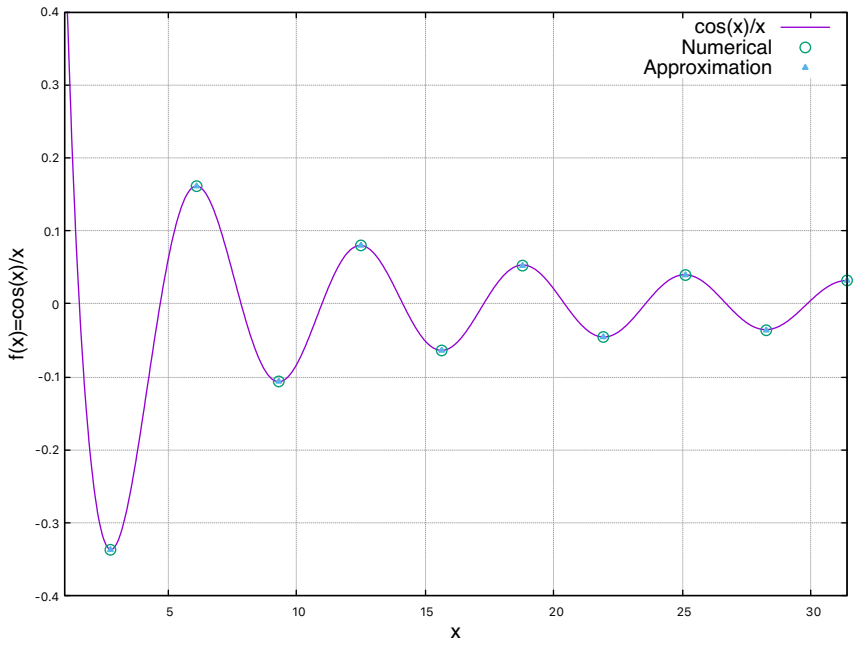

FIG. 5: Plotting of $f(x)$ superposed with the numerical extremum and their approximations.

is satisfied. The numerically obtained values are

$$x_{1,1} = 2.7983860457832299 \tag{45}$$

$$f(x_{1.1}) = 0.33650841691839534, \tag{46}$$

so that

$$y_0 < \frac{1}{0.33650841691839534} \simeq 2.97169387071380169353. \tag{47}$$

Because y_0 is related to the depth of the potential well via $y_0 \to \sqrt{v_0}$, the current consideration corresponds to the "shallow-potential" case, as seen in the structure of a deuteron. Numerical evaluation of the root is made by means of the bisection search with the initial values of $x = 0$ and $x = \pi/2$. The result for the case of $1/y_0 = f(x_{1,1}) = 0.33650841691839534$ is obtained as

$$x^{(0)} = 1.1671646771529784 < y_0 = 2.97169387071380169353, \tag{48}$$

which is the upper limit of $x^{(0)}$ for the situation that only the ground state is possible and that no excited states are allowed. When y_0 becomes larger than the above value, that is, the potential well becomes deeper, the excited states can be allowed in addition to the ground state.

For the above eigenvalue, the other parameter k_0' is evaluated through Eq.(15), which is

$$k_0' = 2.73289060842779431619, \tag{49}$$

and the corresponding energy eigenvalue is given as a square of this value,

$$\mathcal{E} = k_0'^2 = 8.83096446123797713462. \tag{50}$$

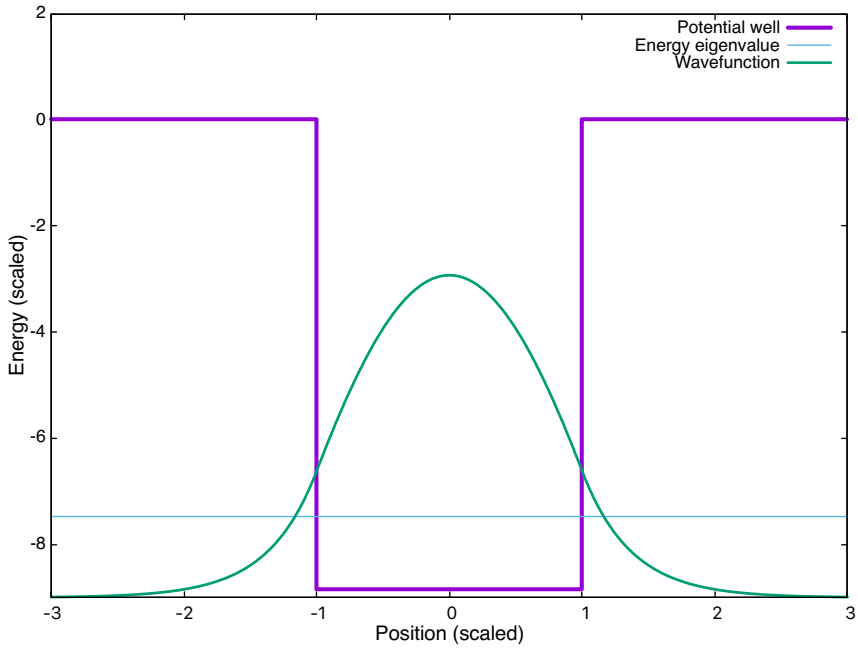

FIG. 6: The ground-state energy $\mathcal{E} = 8.830\cdots$,Eq.(50), and its wave function.

8.2 Excited states

Let us consider an example when $1/y_0$ satisfies the following condition,

$$|f(x_{1,2})| < \frac{1}{y_0} < \frac{1}{\pi}. \tag{51}$$

According to the criteria Eq.(34), this situation allows the single excited state as well as the ground state, that is, two states in total. Each solution can be found in D_0 and D_1, respectively.

Because $f(x_{1,2}) = 0.1612\cdots$ and $1/\pi = 0.3183\cdots$..., let us choose $1/y_0 = 0.2$ as a numerical example. With the bisection search, we find

$$x^{(0)} = 1.3064400083695611 < x^{(1)} = 3.8374671064989316 < y_0 = 5. \tag{52}$$

The corresponding wave numbers k_0' are calculated as

$$k_0' = 4.82630443554305\cdots(\text{ground}), \quad 3.2052841069915\cdots(\text{excited}), \tag{53}$$

so that the scaled energies $\mathcal{E} = k_0'^2$ are

$$\mathcal{E}^{(0)} = -23.2932145045425 \quad \mathcal{E}^{(1)} = -10.2738462065323 \tag{54}$$

The results are plotted in Fig.7.

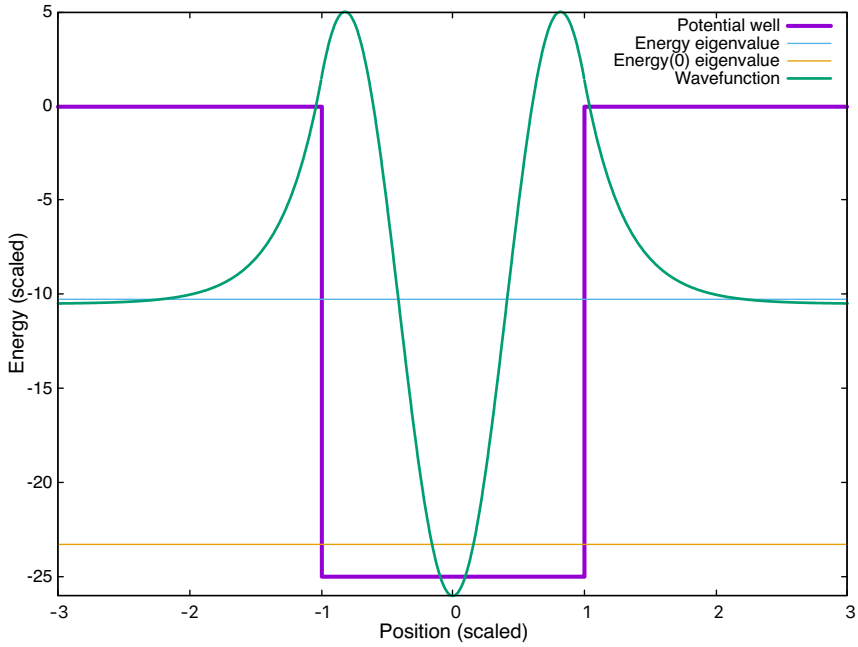

FIG. 7: The first excited and the ground-state energies, Eq.(54), are plotted with a superposition of the excited-state wave function.

9. Eigenvalues of odd solutions

Now, let us turn to the odd solutions of the eigenvalue equation, Eq.(22). For the sake of simplicity, we rewrite the equation.

$$\frac{|\sin x|}{x} = \frac{1}{y_0}, \tag{55}$$

with $y_0 > 0$. The solutions must be contained in the region $U \equiv [0 : y_0]$. To investigate the analytical natures of the left-hand side of the equation, let us introduce the following function,

$$g(x) = \frac{\sin x}{x}. \tag{56}$$

The zeros of this function are

$$x_{z,n} = n\pi. \tag{57}$$

The derivative is

$$g'(x) = -\frac{1}{x^2}\left(\sin x - x\cos x\right), \tag{58}$$

so that the positions of the extrema of $g(x)$ are given as the zeros $x_{e,n}$ of $g'(x)$, which have the asymptotic form for $x \to \infty$,

$$x_{e,n} \simeq \frac{2n+1}{2}\pi, \tag{59}$$

because the second term in $g'(x)$ becomes dominant at large x. However, we already know that this asymptotic expression is insufficient as an approximation to $x_{e,n}$ because $g'(x_{e,n}) \simeq 0$ is not satisfied even to a reasonable accuracy. We thus apply the same treatment as in the even-function case to the present case, that is, we employ an expression

$$x_{e,n} = \frac{2n+1}{2}\pi - \epsilon, \tag{60}$$

with the condition $0 < \epsilon \ll 1$. Inserting this expression to Eq.(58) gives rise to

$$\begin{aligned} g\left(\frac{2n+1}{2}\pi - \epsilon\right) =& (-1)^{n+1}\frac{1}{\left(\frac{2n+1}{2}\pi - \epsilon\right)^2}\left\{\cos\epsilon - \left(\frac{2n+1}{2}\pi - \epsilon\right)\sin\epsilon\right\} \\ \simeq& (-1)^{n+1}\frac{1}{\left(\frac{2n+1}{2}\pi - \epsilon\right)^2}\left\{1 - \frac{1}{2}\epsilon^2 + \cdots - \left(\frac{2n+1}{2}\pi - \epsilon\right)(\epsilon + \cdots)\right\}. \end{aligned} \tag{61}$$

Therefore, in order to fulfill the condition $g'(x_{e,n}) = 0$, the following condition must be imposed.

$$1 - \frac{2n+1}{2}\pi\epsilon + \frac{1}{2}\epsilon^2 \simeq 0. \tag{62}$$

The solution of this quadratic equation reads

$$\epsilon = \frac{2n+1}{2}\left(1 \pm \sqrt{1 - \frac{2}{\left(\frac{2n+1}{2}\pi\right)^2}}\right). \tag{63}$$

We keep only the solution satisfying $\epsilon \ll 1$, which can be approximated to the second order in the Taylor series expansion for the square root.

$$\epsilon \simeq \left(\frac{2n+1}{2}\pi\right)^{-1}\left\{1 + \frac{1}{2}\left(\frac{2n+1}{2}\pi\right)^{-2}\right\}. \tag{64}$$

We thus have expressions for the positions of the extrema $x_{e,n}$ in the following manner.

$$x_{e,n} \simeq \frac{2n+1}{2}\pi - \left(\frac{2n+1}{2}\pi\right)^{-1}, \tag{65}$$

or

$$x_{e,n} \simeq \frac{2n+1}{2}\pi - \left(\frac{2n+1}{2}\pi\right)^{-1} - \frac{1}{2}\left(\frac{2n+1}{2}\pi\right)^{-2}. \tag{66}$$

It should be noted that the above expressions are applicable only to $n > 0$, that is, $n = 0$ must be excluded due to the reason given later.

To satisfy the condition $k_0' > 0$ through Eq.(16), the solutions of Eq.(55) are restricted to certain domains, in the similar fashion to the even-solution case. It is thus convenient to introduce the subdomains F_n in the universal domain U as

$$F_n, \left[(2n+1)\frac{\pi}{2} : (n+1)\pi\right], \ n = 0, 1, 2\cdots. \tag{67}$$

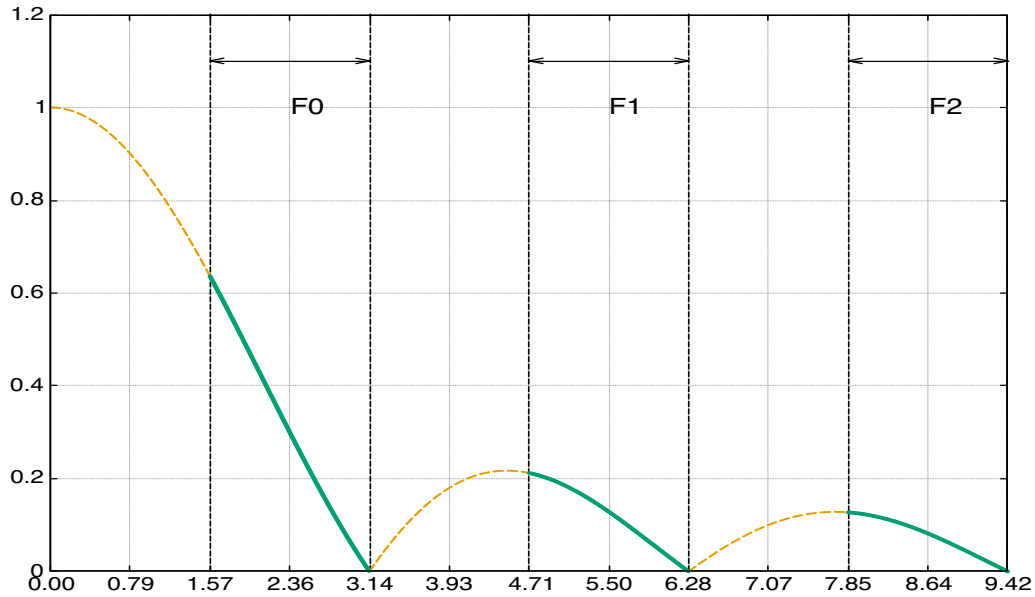

FIG. 8: Plotting of $f(x) = |\sin x|/x$ and the subdomains F_0, F_1, F_2 where the roots of $g(x) - y_0^{-1} = 0$ are possible.

We can demonstrate in a similar way to the even case that the roots of Eq.(55) exist only in these subdomains F_n, and that the function $g(x)$ behaves as a monotonically decreasing function in F_n. Numerical evaluation of the roots can be hence simply carried out by means of the bisection root-search algorithm as in the even-solution case. The convergence is quick and smooth in each F_n, thanks to the property that the extremum $x_{e,n}$ is out of the domains $F^A = \bigoplus_n F_n$, where $F_n \cap F_m = \varnothing$ for $n \neq m$, as shown in the Eqs.(65) and (66).

A special interest can be seen in the relation between the extremum $x_{e,0}$ and the subdomain F_0. In most cases except small n, the extrema are just outside of the subdomain, that is, $x_{e,n} \lesssim \frac{2n+1}{2}\pi$. The smaller n, the greater the deviation $\epsilon_n = \frac{2n+1}{2}\pi - x_{e,n}$. The greatest deviation is seen for $n = 0$, where $x_{e,0} = 0$ hence $\epsilon_0 = \pi/2$. This largeness is the reason why the approximations Eq.(65) and/or Eq.(66) cannot be applicable to the $n = 0$ case. At $n = 1$, the deviation quickly narrows to $\epsilon_1 \simeq 0.212$(first order) $- 0.257$(second order), and the deviations for larger n continues to shrink. Unlike the even-solution case, $g'(0) = 0$ is satisfied and $x = 0$ is qualified as a position

1	2	3	4	5
4.4934094579093316	7.7252518369381562	10.904121659428803	14.066193912831849	17.220755271930276
4.5001823895954960	7.7266576795009669	10.904628605797479	14.06643141089100	17.220885069983172
4.4776665710083101	7.7185519848095803	10.900493047281465	14.063929653270206	17.219210339675033

TABLE III: Numerical values for $x_{e,n}$ for $n = 1, 2, 3, 4, 5$ (upper row), and the approximations, Eq.(65) (middle row) and Eq.(66) (bottom row).

6	7	8	9	10
20.371302959287458	23.519452498689294	26.666054258812771	29.811598790892734	32.956389039822341
20.371381496613076	23.519503583765609	26.666089333609268	29.811623905294212	32.956407635437230
20.370182429351036	23.518602951022121	26.665388148947383	29.811062569096748	32.955948128935454

TABLE IV: Numerical values for $x_{e,n}$ for $n = 6, 7, 8, 9, 10$ (upper row), and the approximations, Eq.(65) (middle row) and Eq.(66) (bottom row).

for a maximum, as demonstrated below.

$$\begin{aligned} g'(\epsilon) =& -\frac{1}{\epsilon^2}\left(\sin\epsilon - \epsilon\cos\epsilon\right) \\ =& -\frac{1}{\epsilon^2}\left(\epsilon - \frac{1}{3!}\epsilon^3 + \cdots - \epsilon\left(1 - \frac{1}{2}\epsilon^2 + \cdots\right)\right) \\ =& -\frac{1}{\epsilon^2}\left(-\frac{1}{3!} - \frac{1}{2}\right)\epsilon^3 + O(\epsilon^2), \end{aligned} \tag{68}$$

which goes to vanish for $\epsilon \to 0$.

Numerical calculations are performed up to $n = 10$ and are compared with the approximations. The results are displayed in Tables III and IV, except the trivial case of $n = 0$.

It is interesting that the the first-order approximation is fairly accurate in comparison with the numerically obtained values. As a result, he additional correction of the second-order term hence brings a larger deviation. See Fig.9.

Let us now calculate the eigenvalues corresponding to the odd solutions by numerically handling Eq.(55).

First of all, there is no solution when

$$\frac{1}{y_0} > g(\pi/2) = \frac{2}{\pi} \tag{69}$$

Next, there is a single solution in F_0 when

$$g(\pi/2) = \frac{2}{\pi} > \frac{1}{y_0} > |g(3\pi/2)| = \frac{2}{3\pi} \tag{70}$$

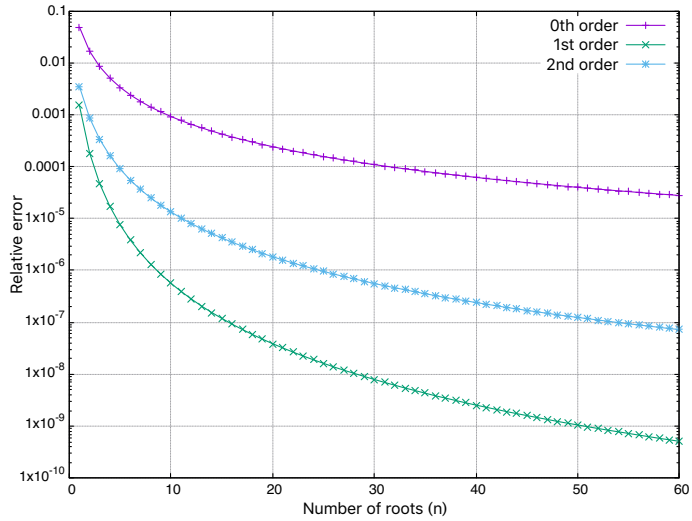

FIG. 9: Relative errors of the three types of approximated $x_{e,n}$ with respect to the numerically obtained values: (i)the zero-th order ($(2n+1)\pi/2$), (ii)the first order, Eq.(65) and (iii) the second order, Eq.(66).

Then, there are two solutions and each solution in F_0 and F_1 respectively when

$$\frac{2}{3\pi} > \frac{1}{y_0} > \frac{2}{5\pi}. \tag{71}$$

Finally, there are n solutions and each solution in $F_0, F_1, \cdots, F_{n-1}$ respectively when

$$\frac{2}{(2n-1)\pi} > \frac{1}{y_0} > \frac{2}{(2n+1)\pi} \tag{72}$$

Let us perform a numerical search for the eigenvalues in the case of

$$\frac{2}{3\pi} > \frac{1}{y_0} = \frac{1}{2\pi} > \frac{2}{5\pi}, \tag{73}$$

which corresponds to the case when there are two solutions ($n = 2$).

Two eigenvalues are calculated as

$$x^{(0)} \to \kappa'^{(0)} = 2.6977996212022219, \tag{74}$$

$$x^{(1)} \to \kappa'^{(1)} = 5.2840797026558413. \tag{75}$$

The corresponding wave numbers are evaluated as

$$k_0'^{(0)} = 5.67453036013334, \tag{76}$$

$$k_0'^{(1)} = 3.39954692573865. \tag{77}$$

Finally, the scaled energies are obtained as

$$\mathcal{E}^{(0)} = -32.200294808075, \tag{78}$$

$$\mathcal{E}^{(1)} = -11.5569193002991. \tag{79}$$

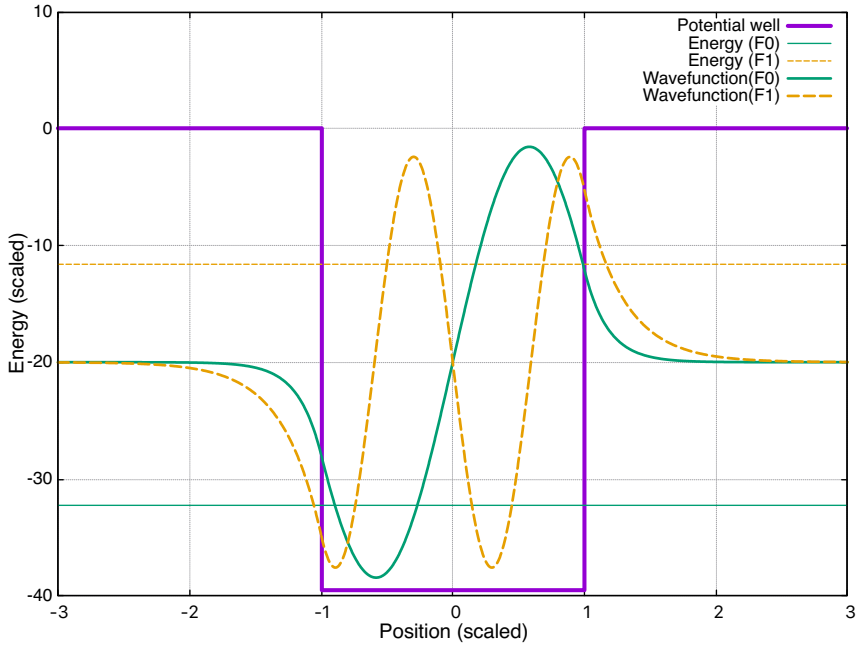

FIG. 10: The first and second excited states and their energies, Eqs.(78) and (79), are plotted.

These numerical results are depicted in Fig.10.

10. Conclusion

The quantum mechanical problem for the one-dimensional potential well was investigated from an analytical and numerical perspectives. The solutions of this problem are widely known and the standard approach is well established. An alternative approach was presented in this paper for an improvement in the numerical algorithm. Although the standard method employs the two-dimensional graphical approach, the eigenvalue equation can be reduced to be a one-dimensional equation in my proposed method. As a result, analytical properties of the root distribution can be easily understood from an intuitive point of view, and the programming can be simplified to a great extent and the numerical accuracy can be improved.

Reference

[1] M. Oi, "Quantum-mechanical rotation of linear rigid body: (0)general properties of rigid bodies", Senshu-university Proceedings of Natural Sciences, No.54 (2023).

[2] The Nobel Foundation, "The Nobel Prize in Chemistry 2023", https://www.nobelprize.org/prizes/chemistry/2023/summary/

[3] P. Ring and P. Schuck, "The nuclear many-body problem", Springer (1980).